Transactions of Tianjin University (2020) 26:142–147
https://doi.org/10.1007/s12209-020-00232-0

RESEARCH ARTICLE

$LaNiO_3$ as a Novel Anode for Lithium-Ion Batteries

Chang Zhang[1] · Cong Wu[1] · Zhiwei Zhang[1] · Yanran Shen[1] · Wei Liu[1]

Received: 12 November 2019 / Revised: 14 December 2019 / Accepted: 23 December 2019 / Published online: 13 January 2020

Abstract
Lithium-ion batteries (LIBs) have been developed for over 30 years; however, existing electrode materials cannot satisfy the increasing requirements of high-energy density, stable cycling, and low cost. Here, we present a perovskite-type $LaNiO_3$ oxide (LNO) as a new negative electrode material. LNO was successfully synthesized by a sol–gel method. The microstructure and electrochemical performance of LNO calcined at various temperatures have been systematically investigated. The LNO electrode shows a high rate capability and long cycling stability. In a C-rate test, a specific capacity of 77 mAh/g was exhibited at 6 C. LNO can also deliver a specific capacity of 92 mAh/g after 200 cycles at 1 C. This paper presents a type of binary metal oxide as a new anode material for high-performance LIBs.

Keywords Lithium-ion batteries · $LaNiO_3$ · Sol–gel method · Perovskite · Electrochemical properties

Introduction

Lithium-ion batteries (LIBs), one of the most remarkable energy storage technologies for the past 30 years, have been widely used for portable electronics and power tools and are now making their way into electric vehicles (EVs) and grid storages [1–4]. Different types of electrode materials have been examined to meet the growing demands of high-energy density and long cycling life for LIBs such as $LiFePO_4$, $LiCoO_2$, $LiNi_{1-x-y}Co_xAl_yO_2$, and $LiNi_{1-x-y}Co_xMn_yO_2$ for cathode materials and graphite, $Li_4Ti_5O_{12}$, Si/C, and P for anode materials [4–10]. However, commercialized graphite anodes show a poor rate capability that limits their application in high C-rate conditions. Moreover, the $Li_4Ti_5O_{12}$ anode exhibits a higher charging/discharging platform, which reduces energy density and impedes its large-scale use.

In addition, metal oxides have gained scientists' attention because of their high specific capacity and have been considered and investigated as alternative anodes in recent years [11–13]. There are three types of electrode reaction mechanisms: alloying–dealloying, intercalation–deintercalation, and conversion (redox) [14, 15]. Jin et al. [11] studied a high-energy density, high-theoretical capacity anode electrode material that comprised Se-based oxides and had a reaction mechanism based on Li–Se alloys. Han et al. [12] reported a new material of KNb_5O_{13} that relied on the intercalation–deintercalation reaction. This type of transition metal oxides has a multidimensional layer structure that can be the host for Li-ion reversible insertion and extraction without destroying the lattice structure. Zhang et al. [13] developed a new material based on the conversion reaction. The new material, $LaCoO_3$, reveals the new reaction mechanism between $LaCoO_3$ and Li metal. Cabana et al. [14] summarized the conversion reactions of approximately 50 electrode materials, including Cr_2O_3, Mn_2O_3, Fe_2O_3, NiO, CuO, and Co_3O_4 monometal oxides. In 1981, Thackeray and Coetzer [16] studied Fe_2O_3 and Fe_3O_4, and some degrees of cyclic reversibility were observed using molten LiCl/KCl electrolytes at a high temperature. However, these types of metallic oxides were not considered alternative electrode materials for LIBs because of their irreversibility at room temperature. Fortunately, at a later point in time, proof was found that several oxides had stable specific capacities that were as much as three times those of carbon materials [15]. Currently, the concept of "conversion reaction" as a new strategy has been widely accepted. Up to now, most of the researches based on "conversion reaction" electrode materials focused on monometal oxides, and several binary metal oxides such as $CoSnO_3$, $NiCo_2O_4$, and $CaSnO_3$ have also been synthesized and investigated [17–19].

✉ Wei Liu
liuwei1@shanghaitech.edu.cn

[1] School of Physical Science and Technology, ShanghaiTech University, Shanghai 201210, China

Here, we report a perovskite-type $LaNiO_3$ oxide (LNO) as a new negative electrode for LIBs. LNO was prepared by a sol–gel method. Calcination temperature was studied, and the microstructure and morphology of the samples were systematically characterized. The rate capability and cycling performance of the LNO electrode were also studied.

Experiment

Synthesis

LNO was prepared via a sol–gel method using lanthanum nitrate, nickel nitrate, and citric acid [20–22]. First, 0.02 mol lanthanum nitrate hexahydrate ($La(NO_3)_3{\cdot}6H_2O$, 99.99%, Aladdin) was dissolved in 40 mL distilled water via magnetic stirring. Then, 0.02 mol nickel nitrate hexahydrate ($Ni(NO_3)_2{\cdot}6H_2O$, 99.99%, Aladdin) was added into the solution. After previous ones were completely dissolved, 0.04 mol citric acid monohydrate ($C_6H_8O_7{\cdot}H_2O$, 99.99%, Aladdin) was added into the solution using a complexing agent. Second, the mixture solution was magnetically stirred and heated with a hotplate (IKA, C-MAG HS 7) at 40 °C for 2 h for the sol formation. The temperature was increased to 120 °C until excess free water evaporated, and then, a brown dry gel was obtained. Subsequently, the temperature was increased to 300 °C and spontaneous ignition occurred, which was named the "Pechini" reaction route. Finally, after slight grinding, the products were calcined at 700 °C and 1100 °C for 8 h in air at a heating rate of 5 °C/min (HF Kejing, KSL-1200X). The products were ground into fine powders for the next step.

Electrode Fabrication

LNO powders, Super P, and polyvinylidene fluoride (PVDF) with a weight ratio of 8:1:1 were mixed and fully ground using a mortar and pestle. The mixture was dispersed in NMP to form slurry, cast-coated onto a copper foil as a current collector, and dried at 80 °C in a vacuum oven overnight. Then, the electrode foil was punched into disks (diameter = 12 mm) as a working electrode in the cell. A lithium foil (diameter = 14 mm) was used as counter/reference electrodes. Celgard 2325 microporous membrane comprising polypropylene/polyethylene/polypropylene (PP/PE/PP) was used as a separator (diameter = 16 mm). Then, the electrolyte was composed of the solution of 1 mol/L $LiPF_6$ in ethylene carbonate (EC) and diethyl carbonate (DEC) with a volume ratio of 1:1. The CR2032 coin cells were assembled in an argon-filled glovebox (Vigor) with O_2 and H_2O content less than 10^{-6}.

Characterization

The crystalline phase structure of the products obtained at various temperatures was determined by X-ray diffractometry (XRD, Bruker D8 Advance, Cu Kα radiation) ranged from 10° to 80° at a scan rate of 6°/min. The microstructure and morphology of the samples were examined with scanning electron microscopy (SEM, JEOL JSM-7800F). Electrochemical impedance spectroscopy (EIS) was performed on an electrochemical workstation (Bio-Logic, VMP-300). The applied AC perturbation signal was 10 mV, and the frequency range was from 7 MHz to 0.1 Hz. The cyclic voltammetry (CV) were performed in an electrochemical workstation with a potential range of 0.01–2.0 V at a scan rate of 0.3 mV/s. The galvanostatic charge and discharge (GCD) of these cells were tested between the cutoff voltage of 0.01 V and 2.0 V at room temperature on a LAND CT2001A battery testing system.

Results and Discussion

Figure 1 shows the crystalline phase structure of the ABO_3-type LNO. The larger La^{3+} cation occupies site A, the smaller Ni^{3+} occupies site B, and the model drawn by the white dashed line represents a unit cell [22]. The XRD patterns of LNO calcined at various temperatures are given in Fig. 2. The XRD patterns of LNO-700 show that several sharp peaks exist at 23.2°, 32.9°, 40.7°, 41.3°, 47.4°, and 58.7°, which belong to the (100), (110), (021), (003), (200), and (122) crystal faces, respectively. These findings reveal that the product is a perovskite-type $LaNiO_3$ (PDF# 34-1028) without related impurity phase. As the calcining temperature increased, the strongest peak of (110) crystal face separates into three peaks, namely (117), (020), and

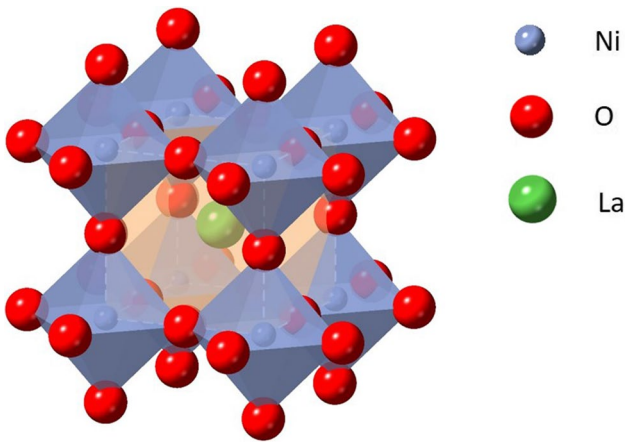

Fig. 1 Crystal structure of the perovskite-type LNO

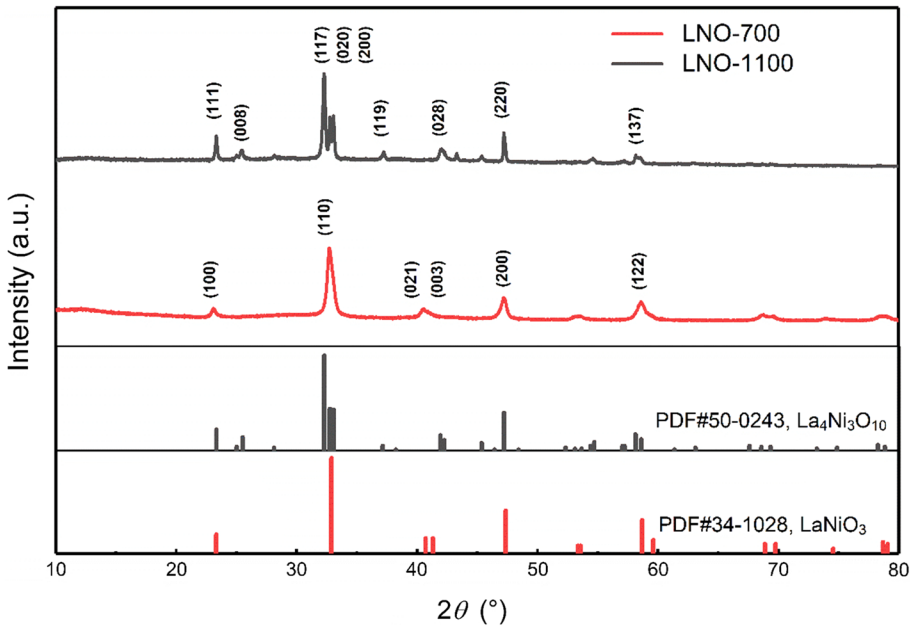

Fig. 2 XRD patterns of the as-prepared LNO samples calcined at 700 °C and 1100 °C

(200). The product that calcined at 1100 °C transformed into an orthorhombic $La_3Ni_4O_{10}$ (PDF# 50-0243) [22–24].

The micromorphology and electrochemical performance of the LNO powders calcined at various temperatures were studied. Figure 3 shows the SEM images of the LNO samples calcined at 700 °C (LNO-700) and 1100 °C (LNO-1100). As shown in Fig. 3a, b, the average size of the LNO-700 particles is ~ 300 nm. Figure 3c, d exhibits that the particle size grows to ~ 500 nm when the calcination temperature is 1100 °C. Evidently, LNO-700 has a more homogeneous grain diameter and larger specific surface area, which may be among the reasons for its better electrochemical performances.

Next, the electrochemical performances of LNO were evaluated. The previous research [13, 20] has proposed the following reaction mechanism for the conversion reaction of LNO

$$2LaNiO_3 + 2Li \rightarrow Li_2O + La_2O_3 + 2NiO \quad (1)$$

$$NiO + 2Li \rightleftharpoons Ni + Li_2O \quad (2)$$

Accordingly, the theoretical specific capacity of LNO was calculated as 218 mAh/g. Figure 4a shows the CV curves of LNO-700 at a scan rate of 0.3 mV s^{-1}. In the first scanning cycle, the LNO electrode exhibits a large and broad reduction peak, ranging from 0.8 to 0.3 V, and the peak disappears in the next cycling. This can be attributed to the formation of the solid electrolyte interface (SEI) layer and the reduction of Ni^{3+} to Ni^{2+} described in Eq. (1), which is verified by the GCD curves shown in Fig. 4b. The first discharging process had a plateau from 0.8 to 0.3 V. From the second scanning of CV in Fig. 4a, there are an oxidation peak at ~ 1.6 V and a reduction peak at ~ 1.0 V, which reveal that it is a reversible reaction, as described in Eq. (2). Moreover, there are corresponding plateaus in the GCD curves.

To further study the electrochemical behaviors of the Li|LNO half cells, electrochemical impedance spectroscopy (EIS) measurements were taken before cycling in the frequency range from 7 MHz to 0.1 Hz (Fig. 5a). The inset in Fig. 5a shows the equivalent circuit. As can be seen, the EIS spectra comprise three parts: the intersection with the real axis in the high-frequency region, a semicircle in the middle-frequency region, and a sloped straight line in the low-frequency region. The intersection corresponds to the electrolyte resistance (R_b), and the values of LNO-700 and LNO-1100 are 3.4 Ω and 3.7 Ω, respectively. The semicircle indicates the overlapping of the interfacial resistance (R_1) and charge transfer resistance (R_{ct}). The straight line is attributed to the Li-ion Warburg diffusion process in the electrode. Moreover, the Li-ion diffusion coefficient (D_{Li+}) can be calculated using the following equation [25].

$$D = \frac{R^2T^2}{2n^4F^4A^2c^2\sigma^2} \quad (3)$$

$$Z_{re} = R_{ct} + R_b + \sigma\omega^{-1/2} \quad (4)$$

where R is the gas constant; T is the absolute temperature; n is the number of the electrons per molecule attending the electronic transfer reaction; F is the Faraday constant; A is the surface area of the LNO electrode; c is the concentration of Li-ion in the electrode; and σ is the Warburg factor that can be obtained from the slope (Fig. 5b) of the linear

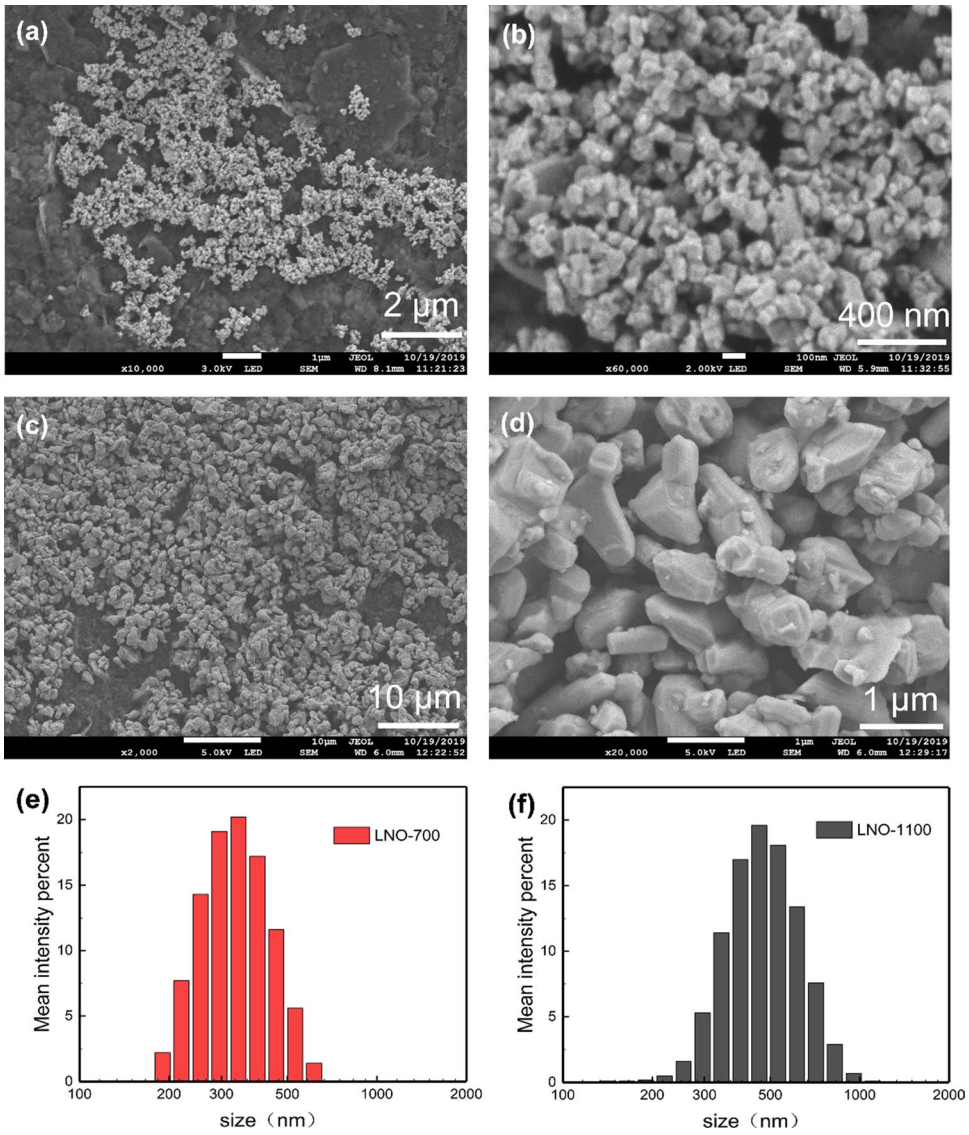

Fig. 3 SEM images of LNO-700 (**a**, **b**) and LNO-1100 (**c**, **d**); particle size distribution of **e** LNO-700 and **f** LNO-1100

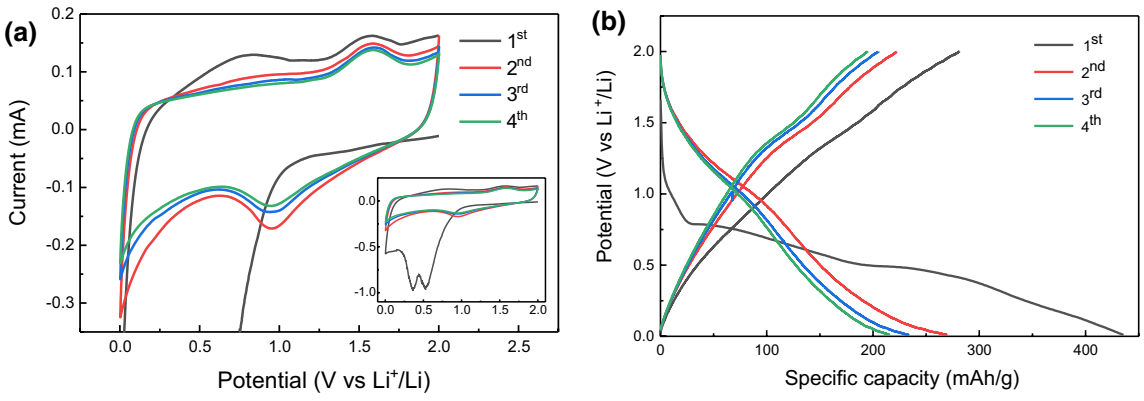

Fig. 4 Electrochemical performances of LilLNO-700 half cells between the cutoff voltage of 0.01 V and 2.0 V. **a** CV curves at a scan rate of 0.3 mV/s and **b** GCD curves at current density of 20 mA/g

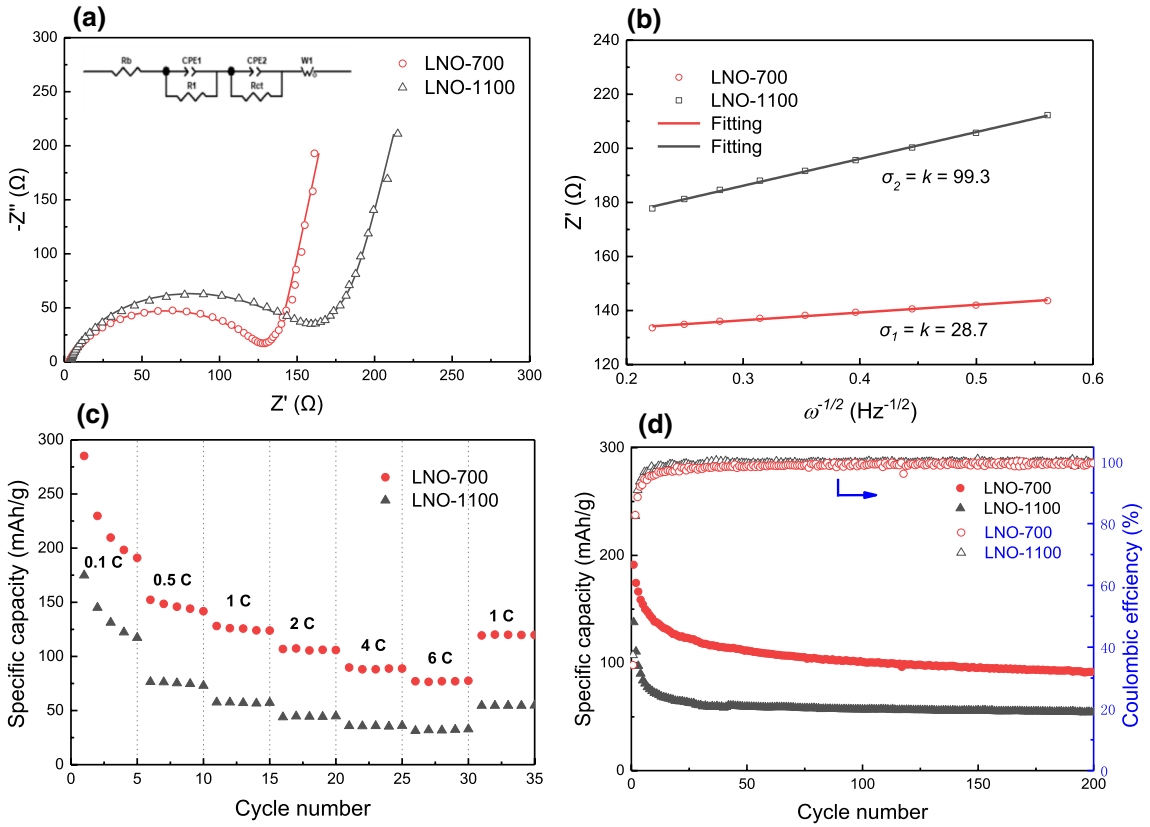

Fig. 5 **a** Nyquist plots, **b** plots of Z' versus $\omega^{-1/2}$, **c** rate capability, and **d** cycling performances of LilLNO-700 and LilLNO-1100 half cells. The inset of **a** shows the equivalent circuit

fitting of the real part of the impedance spectra (Z_{re}) versus the reciprocal square root of the angular frequency ($\omega^{-1/2}$), as shown in Eq. (4). The sloped straight line of LNO-1100 ($\sigma_2 = k = 99.3$) is considerably steeper than that of LNO-700 ($\sigma_1 = k = 28.7$). By putting σ_1 and σ_2 into Eq. (3), we found that $D_1 = 2.12 \times 10^{-15}$ cm^2/s and $D_2 = 1.77 \times 10^{-16}$ cm^2/s. Because $D_1/D_2 = 12$, the diffusion velocity of Li-ion is faster than that in the LNO-700 electrode system.

Generally, the rate capability decides the power density in the batteries. Therefore, the electrode materials should deliver a higher actual capacity at a high C-rate. As shown in Fig. 5c, the LNO-700 electrode exhibits a specific capacity of 152 mAh/g at 0.5 C, 124 mAh/g at 1 C, 107 mAh/g at 2 C, 89 mAh/g at 4 C, and 77 mAh/g at 6 C. When the C-rate returns to 1 C, the specific capacity is 120 mAh/g. Moreover, the LNO-1100 electrode shows a specific capacity of 76 mAh/g at 0.5 C, 56 mAh/g at 1 C, 44 mAh/g at 2 C, 36 mAh/g at 4 C, 32 mAh/g at 6 C, and 54 mAh/g at 1 C. Evidently, the rate capability of LNO-700 is considerably higher than that of LNO-1100, which is attributed to more uniformly distributed grains and smaller grain size.

The cycling performance of LNO-700 and LNO-1100 at 1 C is displayed in Fig. 5d. Compared with LNO-1100, LNO-700 indicates improved performance. The specific capacity presents a fast decay in the first five cycles and then gradually becomes stable. The reason for this phenomenon can be attributed to the irreversible redox reaction described in Eq. (1) and other side reactions. The cycling performance of the LNO electrodes is stable after 30 cycles with a specific capacity of 122 mAh/g. In addition, LNO-700 can deliver a high specific capacity of 92 mAh/g after 200 cycles at 1 C with a capacity retention of 75.4% compared with that of the 30th cycle. Each cycle has a coulombic efficiency close to 99.8%, indicating a stable discharge/charge cycle.

Conclusions

Here, we report a perovskite-type $LaNiO_3$ as a novel electrode material for LIBs. Perovskite-type LNO was successfully fabricated by a sol–gel method, and LNO powders with different grain diameters were obtained at calcination temperatures of 700 °C and 1100 °C. Surface morphology and crystalline phase structure were measured via SEM and XRD, and the electrochemical performances were systematically investigated via CV, EIS, and GCD. LNO-700 shows a higher specific capacity and rate capability than those of LNO-1100. A high specific capacity of 77 mAh/g

was obtained for LNO-700 at a high rate of 6 C. In addition, the LNO-700 anode delivered a high specific capacity of 92 mAh/g after 200 cycles at 1 C.

Acknowledgements This work was supported by the National Natural Science Foundations of China (No. 21805185) and ShanghaiTech University Start-Up Funding.

References

1. Armand M, Tarascon JM (2008) Building better batteries. Nature 451(7179):652–657
2. Liu J, Bao ZN, Cui Y et al (2019) Pathways for practical high-energy long-cycling lithium metal batteries. Nat Energy 4(3):180–186
3. Wu XS, Xia SX, Huang YQ et al (2019) High-performance, low-cost, and dense-structure electrodes with high mass loading for lithium-ion batteries. Adv Funct Mater 29(34):1903961
4. Billaud J, Bouville F, Magrini T et al (2016) Magnetically aligned graphite electrodes for high-rate performance Li-ion batteries. Nat Energy 1(8):16097
5. Ferg E (1994) Spinel anodes for lithium-ion batteries. J Electrochem Soc 141(11):L147
6. Padhi AK (1997) Phospho-olivines as positive-electrode materials for rechargeable lithium batteries. J Electrochem Soc 144(4):1188
7. Chen WH, Li YY, Yang D et al (2016) Controlled synthesis of spherical hierarchical $LiNi_{1-x-y}Co_xAl_yO_2$ ($0<x$, $y<0.2$) via a novel cation exchange process as cathode materials for high-performance lithium batteries. Electrochim Acta 190:932–938
8. Sun Y, Wang L, Li Y et al (2019) Design of red phosphorus nanostructured electrode for fast-charging lithium-ion batteries with high energy density. Joule 3:1080–1093
9. Li XL, Meduri P, Chen XL et al (2012) Hollow core–shell structured porous Si–C nanocomposites for Li-ion battery anodes. J Mater Chem 22(22):11014
10. Zhao L, Hu YS, Li H et al (2011) Porous $Li_4Ti_5O_{12}$ coated with N-doped carbon from ionic liquids for Li-ion batteries. Adv Mater 23(11):1385–1388
11. Jin J, Tian XC, Srikanth N et al (2017) Advances and challenges of nanostructured electrodes for Li–Se batteries. J Mater Chem A 5(21):10110–10126
12. Han JT, Liu DQ, Song SH et al (2009) Lithium ion intercalation performance of niobium oxides: $KNb_5O_{13}$and $K_6Nb_{10.8}O_{30}$. Chem Mater 21(20):4753–4755
13. Zhang DW, Xie S, Chen CH (2005) Electrochemical reactions between perovskite-type $LaCoO_3$ and lithium. J Electroceram 15(2):109–117
14. Cabana J, Monconduit L, Larcher D et al (2010) Beyond intercalation-based Li-ion batteries: the state of the art and challenges of electrode materials reacting through conversion reactions. Adv Mater 22(35):E170–E192
15. Reddy MV, Subba Rao GV, Chowdari BV (2013) Metal oxides and oxysalts as anode materials for Li ion batteries. Chem Rev 113:5364–5457
16. Thackeray MM, Coetzer J (1981) A preliminary investigation of the electrochemical performance of α-Fe_2O_3 and Fe_3O_4 cathodes in high-temperature cells. Mater Res Bull 16(5):591–597
17. Leng XN, Shao Y, Wu LB et al (2016) A unique porous architecture built by ultrathin wrinkled $NiCoO_2$/rGO/$NiCoO_2$ sandwich nanosheets for pseudocapacitance and Li ion storage. J Mater Chem A 4(26):10304–10313
18. Sharma Y, Sharma N, Subba Rao GV et al (2008) Studies on nano-CaO SnO_2 and nano-$CaSnO_3$ as anodes for Li-ion batteries. Chem Mater 20(21):6829–6839
19. Huang J, Ma YT, Xie QS et al (2018) 3D graphene encapsulated hollow $CoSnO_3$ nanoboxes as a high initial coulombic efficiency and lithium storage capacity anode. Small 14(10):1703513
20. Bannikov DO, Cherepanov VA (2006) Thermodynamic properties of complex oxides in the La–Ni–O system. J Solid State Chem 179(8):2721–2727
21. Wang YP, Zhu JW, Yang XJ et al (2006) Preparation and characterization of $LaNiO_3$ nanocrystals. Mater Res Bull 41(8):1565–1570
22. Zhang J, Zhao YB, Zhao X et al (2015) Porous perovskite $LaNiO_3$ nanocubes as cathode catalysts for Li–O_2 batteries with low charge potential. Sci Rep 4:6005
23. Özbay N, Şahin RZY (2017) Preparation and characterization of $LaMnO_3$ and $LaNiO_3$ perovskite type oxides by the hydrothermal synthesis method. In: MRS Proceedings, Istanbul, Turkey
24. Sun Y, Kotiuga M, Lim D et al (2018) Strongly correlated perovskite lithium ion shuttles. Proc Natl Acad Sci USA 115:9672–9677
25. Nie L, Li YF, Chen SJ et al (2019) Biofilm nanofiber-coated separators for dendrite-free lithium metal anode and ultrahigh-rate lithium batteries. ACS Appl Mater Interfaces 11(35):323–373

Dr. Wei Liu received her BS in materials physics from Beijing Normal University in 2008 and Ph.D. in materials science and engineering from Tsinghua University in 2013. She visited the University of Tokyo in 2010–2011. From 2013 to 2017, she was a postdoctoral scholar at Stanford University. She joined ShanghaiTech University as an assistant professor in 2017. Her research interests cover the area of solid-state ionics and nanotechnology, with a focus on lithium batteries, aiming at increasing the energy density and safety of the batteries. She has more than 60 scientific publications. As the first author or corresponding author, she has published 27 papers in journals including Nature Energy, Nature Commun, Sci Adv, Chem, Adv Mater, JACS, Nano Lett, etc. She is also the peer reviewer of 30 journals such as Nature Commun, Joule and Nano Lett.